Experimental Geometry

Overview

The experimental geometry was designed in order to provide initial turbulent boundary layer (TBL) growth under nominally zero pressure gradient (ZPG) conditions followed by the imposition of an adverse pressure gradient (APG), that is fully adjustable, over a smooth backward facing ramp geometry. In this manner, the streamwise extent of the flow separation could be controlled with a fixed ramp geometry. An additional requirement for the experiment was to provide a turbulent flow whose statistical quantities were homogeneous in the spanwise direction. In the following sections the experimental geometry designed to achieve these objectives is described.

Figures 1 - 4 present schematics and images of the model geometry for the APG TBL experiments installed in the Notre Dame Mach 0.6 wind tunnel facility. Figure 1 shows a CAD model of the test section installed in the wind tunnel. Key elements of the experimental geometry are labeled in Figure 2 and discussed in more detail in the subsequent sections after a brief overview of their relation to one another is presented. Figure 3 presents some of the relevant dimensions of the ramp and boundary layer development plate via a CAD drawing. Finally, a photograph of the ramp model is shown in Figure 4 which highlights the size of the geometry and provides a reference for the coordinate systems that are used in this work.

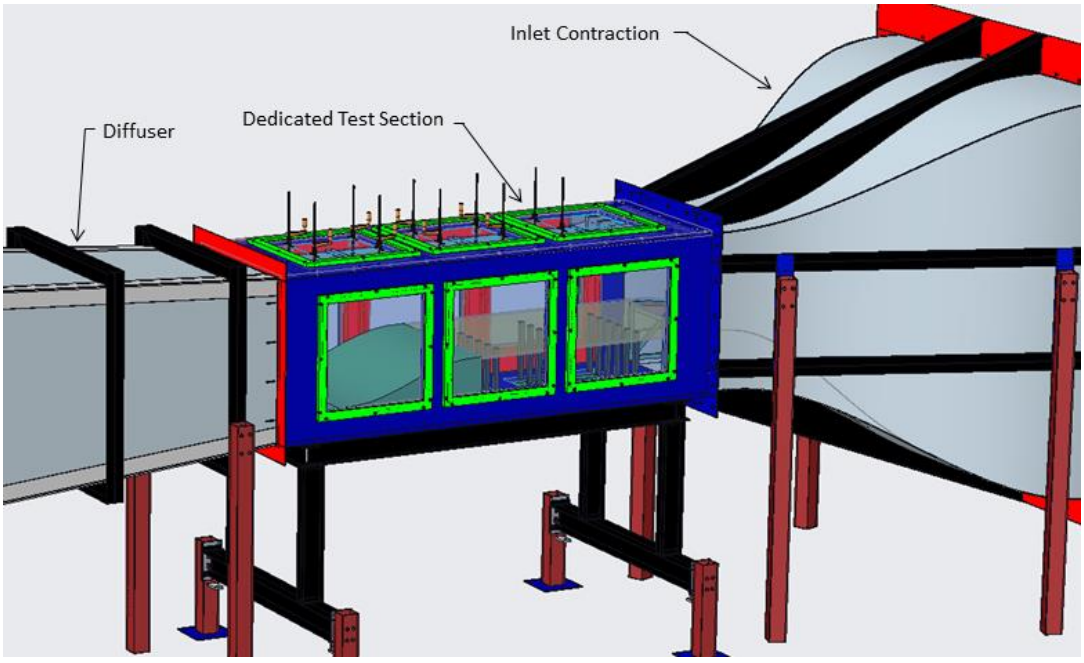

Figure 1. Schematic drawing of the model geometry installed in the Notre Dame Mach 0.6 wind tunnel test section. View is looking from the outer wind tunnel loop.

Important features of the experiment are highlighted in Figure 2 and will be briefly discussed here. On the lower half of the wind tunnel contraction an internal inlet contour is installed. The contour brings the flow smoothly from the wind tunnel inlet contraction up to a flat

boundary layer development plate. The boundary layer development plate allows a uniform boundary layer to grow before reaching the ramp. At the termination of the boundary layer development plate is the ramp geometry, the focus of this experiment. Downstream of the ramp the flow smoothly transitions into the diffuser via removable contours installed on the diffuser floor. The intent of the design is to allow continuous smooth transition from the wind tunnel inlet to the diffuser.

On the upper half of the test section a top wall inlet contour smoothly transitions the flow from the inlet onto a flexible top wall insert. This flexible insert covers most of the test section and acts as a false ceiling. It features two rows of turnbuckles that allow a continuous modification of the streamwise pressure gradient. At the end of this flexible insert (which roughly corresponds to the end of the test section) is a hinge assembly that transitions the flexible ceiling into the diffuser.

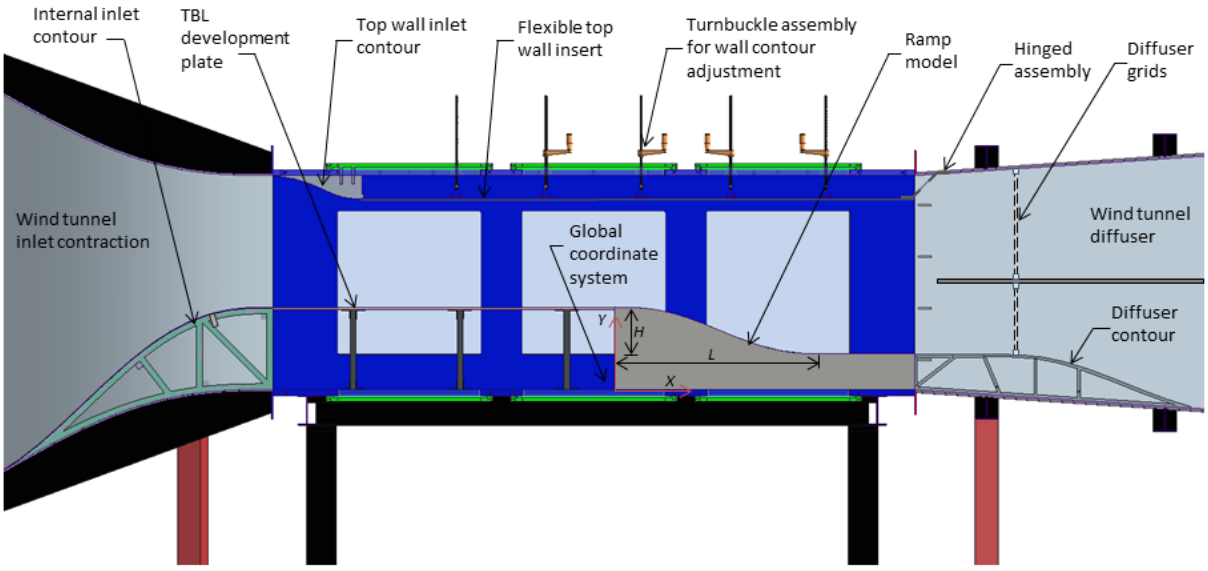

Figure 2 Labeled schematic drawing of the test section and model geometry. View is looking from the inner wind tunnel loop and flow is from left to right.

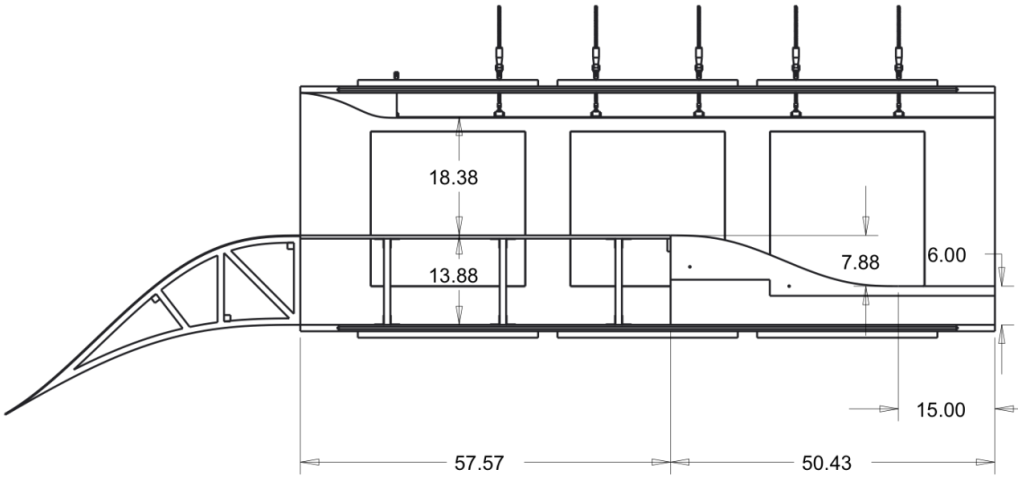

Figure 3 Schematic drawing of the test section and model geometry with dimensions. Units are in inches.

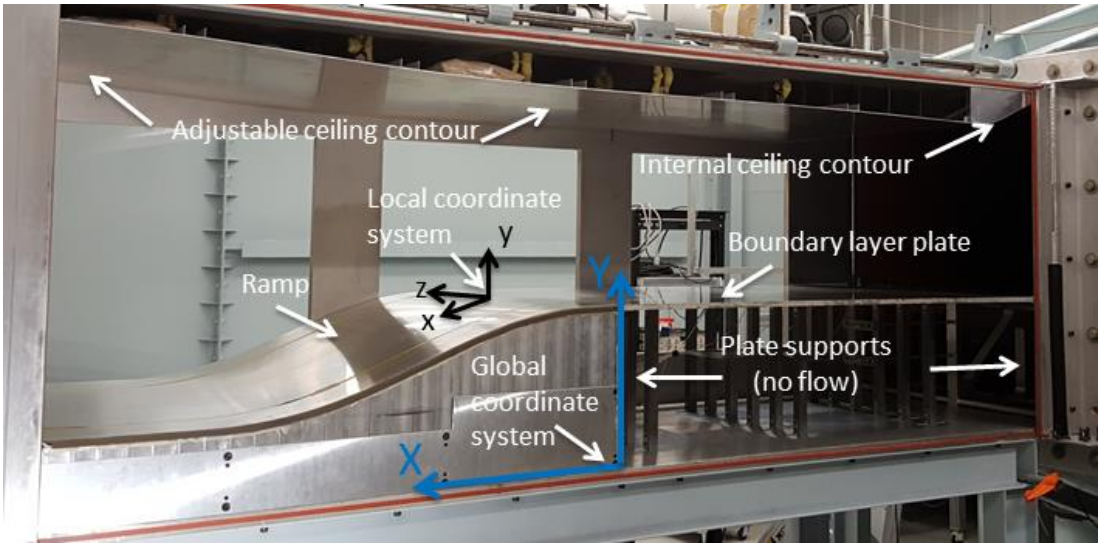

Figure 4 Photograph of the test section model with the sidewall door removed. Note that the sidewall door absent in this photograph is the adjustable one. View is looking from the outer wind tunnel loop and flow is from right to left.

Coordinate Systems

There are two primary right-hand Cartesian coordinate systems used in the data collection and data presentation of this experiment: the global and the local coordinate systems, both shown schematically in Figures 5 & 6. The global coordinate system (X,Y,Z) has its origin at the start of the ramp, and bottom and mid-span of the test section. It is used to represent the physical geometry and the start of each LDV profile. The local coordinate system (x,y,z) is different for each ramp location and has the same spanwise, z, coordinate as the global coordinate system; however, its other two axes are locally wall-normal, y, and wall-tangent, x, oriented. The origin of the local coordinate system is on the surface of the ramp geometry and is defined by a single value of the streamwise global variable, X, or the surface streamwise coordinate, x_s. The angle θ as given for each local coordinate system is defined as the wall-parallel direction, x, rotated counter-clockwise into the tunnel streamwise direction, X. It is primarily used to convert the local flow values from their native locally collected coordinate system to the global coordinate system.

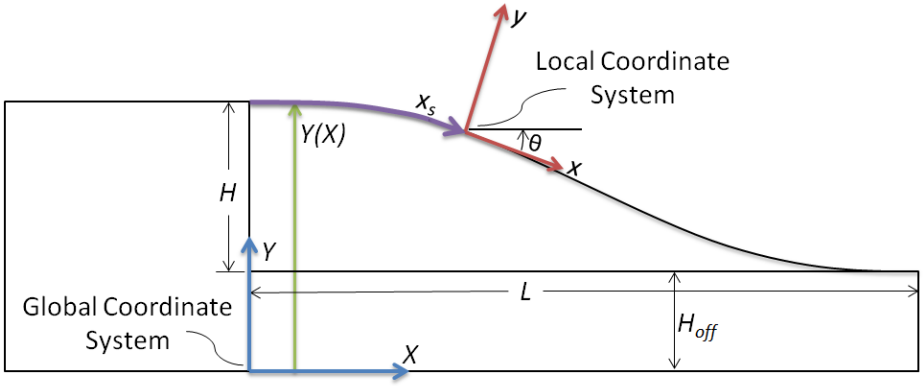

Figure 5 Side view schematic of the global (X,Y,Z) and local (x,y,z) coordinate systems with respect to the ramp geometry.

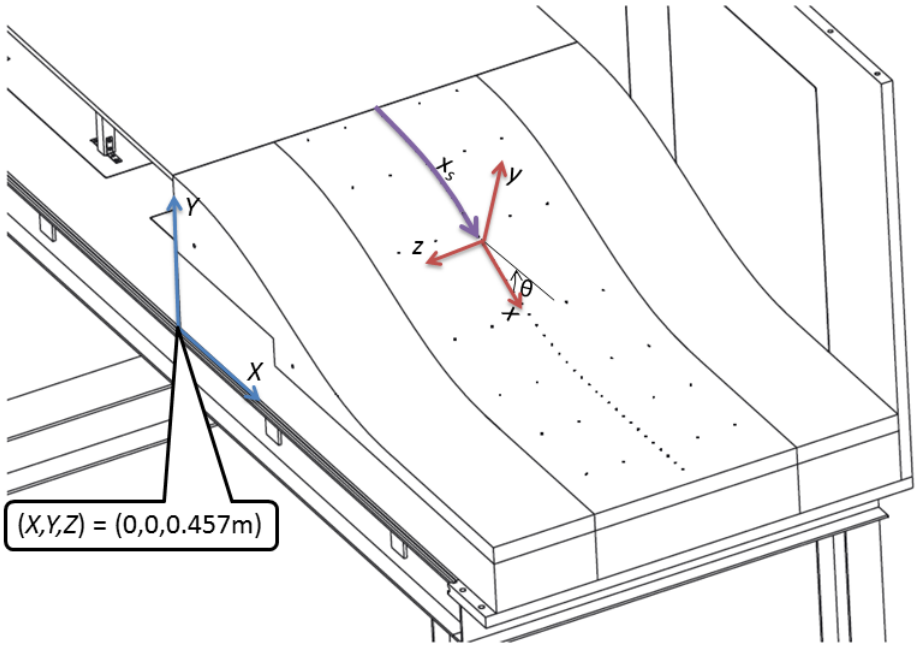

Figure 6 Schematic showing both the streamwise and multiple spanwise static pressure taps on the convex ramp surface and the global (X,Y,Z) and local (x,y,z) coordinate systems.

Ramp Model Geometry

The ramp geometry for these experiments was designed in partnership with the CFD group at NASA Langley Research Center. The selected ramp geometry is a fifth-order polynomial contour with zero first and second derivative end conditions at both upstream and downstream ends of the geometry. It is given by the following parametric form,

$$Y(X) = a_1 + a_2X^3 + a_3X^4 + a_4X^5 \tag{1}$$

where the X denotes the streamwise distance from the end of the boundary layer development plate and $Y(X)$ is the height of the ramp, both in the global coordinate system (see Figures 2 & 5). The constants are given in terms of the ramp length, L = 0.9 m, the ramp height, H = 0.2 m, and the vertical offset, H_{off} = 0.152 m (6 in), as follows:

$$a_1 = \left(H + H_{off}\right), \quad a_2 = -10H/L^3, \quad a_3 = 15H/L^4, \quad a_4 = -6H/L^5 \tag{2}$$

The ramp model, shown in Figure 7, extends the entire width of the test section. It was fabricated in three spanwise sections, each machined in-house from two aluminum blocks, toleranced within 0.025 mm (0.001 in), then welded together. The three sections were bolted together, and its surface given a polished finish so that the seams are undetectable. Note that in addition to the contoured section of the ramp, there is a flat section downstream of the ramp that has a length of 0.381 m (15.0 in). This is manufactured as part of the ramp model and provides the flow with a recovery region prior to entering the wind tunnel diffuser.

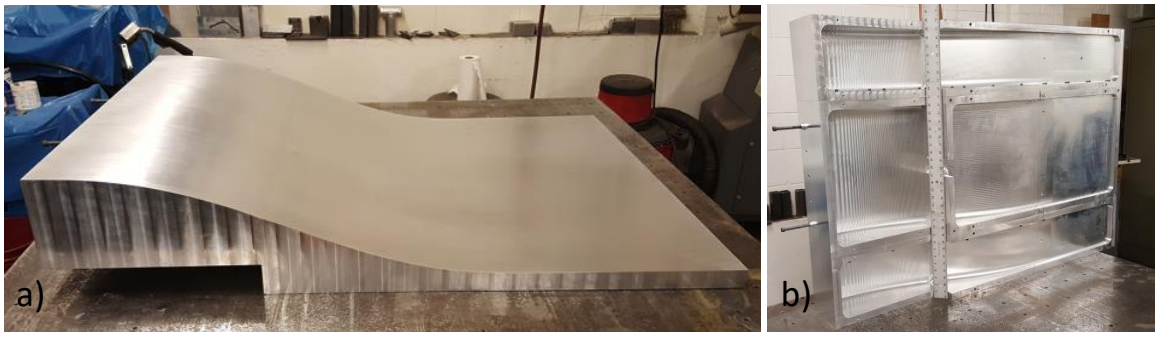

Figure 7 Photographs of the assembled ramp model just after polishing. Top view of the ramp a) and bottom view showing the three separate sections bolted together b).

The boundary layer development plate and ramp together contain a total of 89 surface pressure taps, 61 in the streamwise direction along the central axis, Z = 0, and the remainder in 7 different spanwise arrays along the ramp. See Appendix 1 for tabular data providing each pressure tap location. All pressure taps are confined to central section of the ramp geometry and were drilled wall-normal using a 5-axis CNC milling machine. Scanivalve 063 stainless steel tubulations, each 25.4 mm (1 in) in length with an internal diameter of 1.1 mm (0.0425 in) were superglued flush in the holes. The tubulations were then connected to the pressure transducer via 063 urethane tubing and three separate 31-port circular connectors, both from Scanivalve. The tubulations and tubing are shown in Figure 8 and the pressure tap locations and ramp model sections are highlighted schematically in Figure 6.

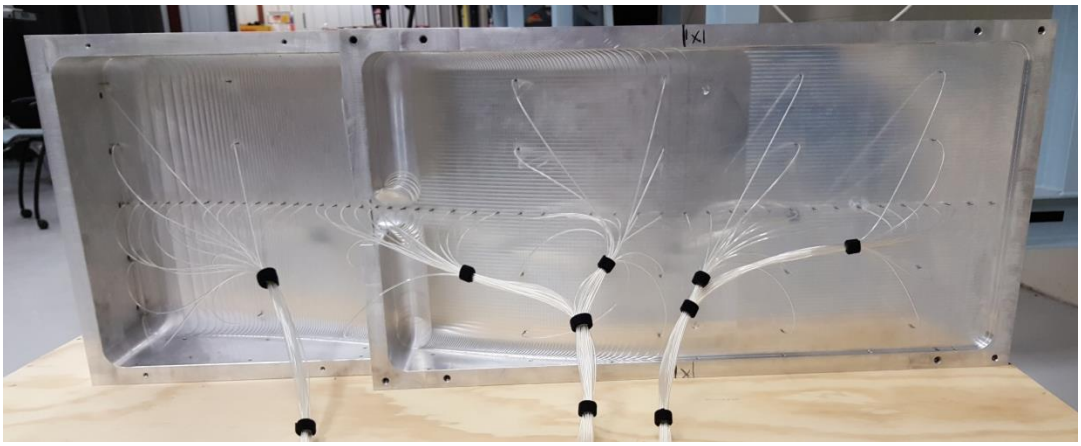

Figure 8 Underside view of the central section of the ramp model showing pressure tubulations and tubing.

The ramp is placed 0.152 m (6in) above the test section floor to allow optical access along its downstream side. To provide this offset, a supporting structure was fabricated out of aluminum and is shown in Figure 9.

Figure 9 Supporting structure for ramp model that provides the necessary 0.152 m (6 in) of vertical offset required for optical access to the recovery region.

Internal Inlet Contour

The internal inlet contour, shown in Figures 2 & 10, is a removable wind tunnel contraction insert, fabricated with a zero derivative end condition to smoothly bring the flow from the wind tunnel inlet contraction up to the leading edge of the flat boundary layer development plate. It consists of two symmetrical inserts each installed on the lower surface of the wind tunnel contraction and bolted to each other and the legs of the boundary layer development plate. Each frame is constructed from aluminum and covered with a 6.35 mm (0.25 in) flexible plastic sheet. Once installed, aluminum foil ducting tape is used to completely seal all internal edges to prevent the front edge from lifting up and allowing airflow to pass underneath the boundary layer development plate. Figure 10 b) shows an in-process photograph of the ducting tape being installed.

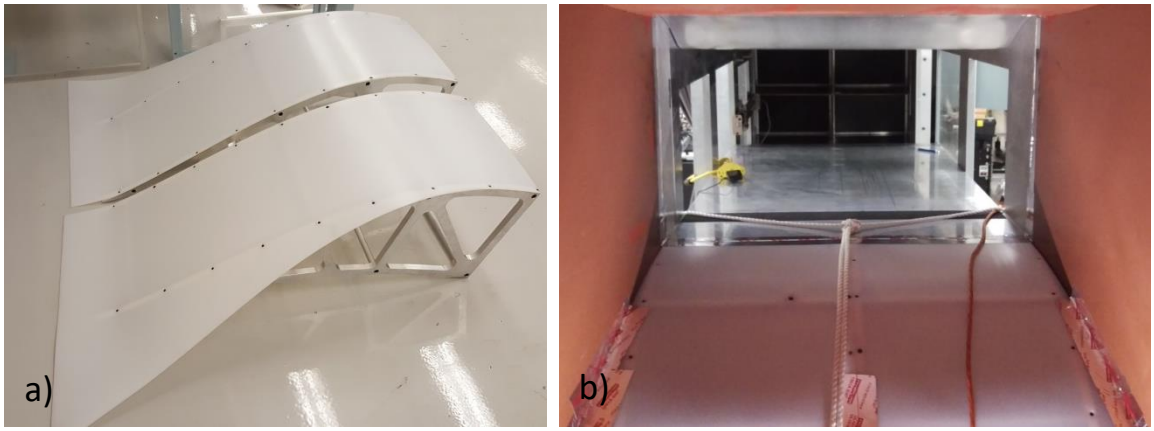

Figure 10 Internal inlet contour sections a) and installed in the wind tunnel contraction b).

Particle Seeding Manifold

The bulk of the experiments are conducted non-intrusively using laser Doppler velocimetry (LDV) which requires the flow be seeded. Di-Ethyl-Hexyl-Sebacot (DEHS) particles of nominally

1 micron diameter were used to seed the flow. In order to minimize the required seeding volume, it was necessary to modify a section of the internal inlet contour to accept a seeding manifold so that localized seeding could be achieved. The internal inlet contour on the –z (spanwise) axis was modified by installing a manifold, shown in Figure 11, that would allow wall-normal particle seeding at the required spanwise locations. The manifold consisted of eight flush-mounted tubes of 9.53 mm (3/8” in) diameter installed 0.24 m (9.5 in) upstream of the test section. Figure 11 a) shows the flush-mounted manifold from the top, airflow side. Internally, the tubes were paired off via a y-connector as shown in Figure 11 b). This system was designed such that by supplying particles to one tube they would eventually exit the manifold straddling the spanwise location of the desired LDV profile. This allowed the seeding to be concentrated only where necessary for each run.

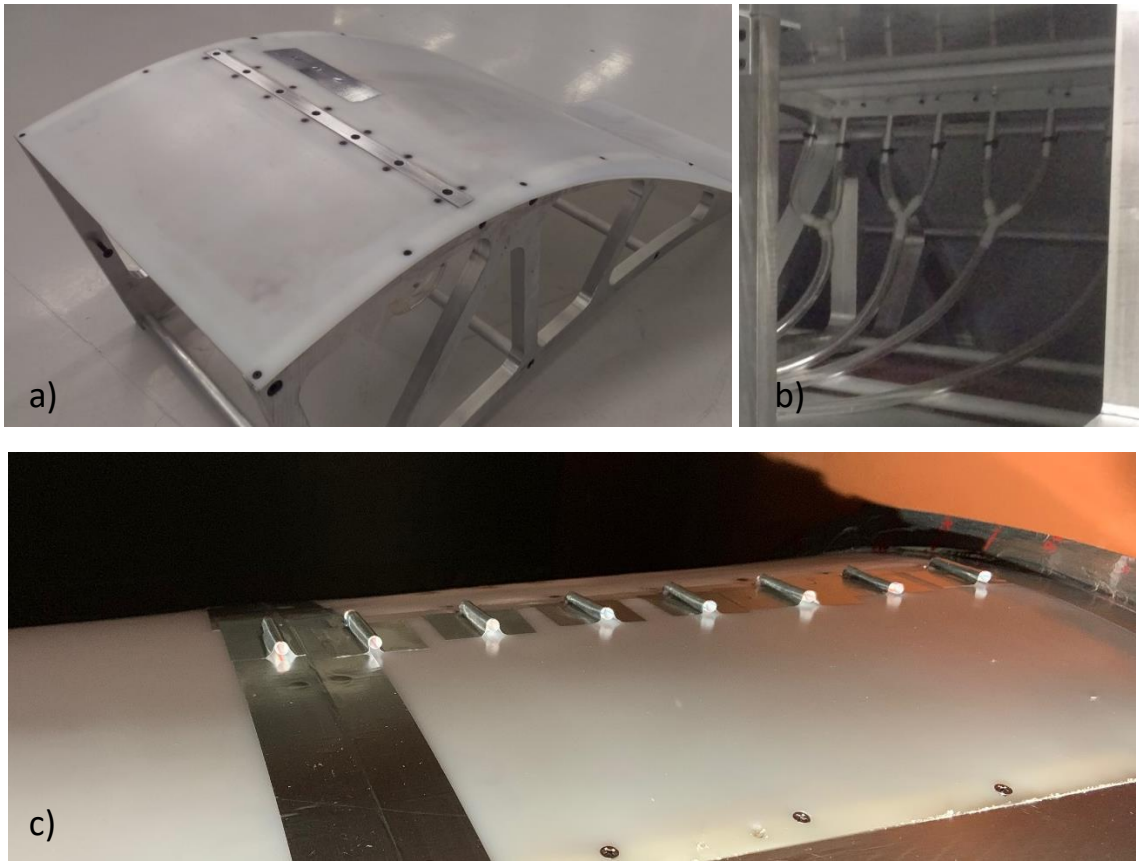

Figure 11 Nearside internal inlet contour modified with a particle seeding manifold to allow localized seeding of the upstream boundary layer. Top view (a) showing flush mounting, internal view (b) showing tubing and y-connectors, and top view (c) showing modified seeding tubes.

An additional modification to the seeding manifold was made prior to making LDV measurements in the recovery region of Case B and all LDV data for Case C. This modification was necessary to keep LDV data acquisition at an acceptable rate and consisted of installing downstream facing straws in the manifold tube openings. Figure 11 c) shows the modified seeding manifold with the straws and can be compared to the original flush-mounted seeding manifold shown in Figure 11 a). The downstream facing tubes increased the concentration of airborne

seeding particle, which prior were collecting on the surface, significantly increasing the LDV data rate. While this modification acted as a physical obstruction in the flow, it occurred in the favorable pressure gradient region and sufficiently far upstream to not adversely affect the experiment. This was determined by taking comparison LDV profiles downstream in the recovery region of Case B using both seeding manifolds with the difference being deemed negligible. In addition, hot-wire boundary layer profiles were taken upstream at X = -0.678 m both with and without the modified seeding method installed. Figure 12 shows the comparison profiles which agree quite well with one another, again, indicating a negligible difference in flow conditions for each seeding method. For more discussion on the particle seeding, see the LDV documentation.

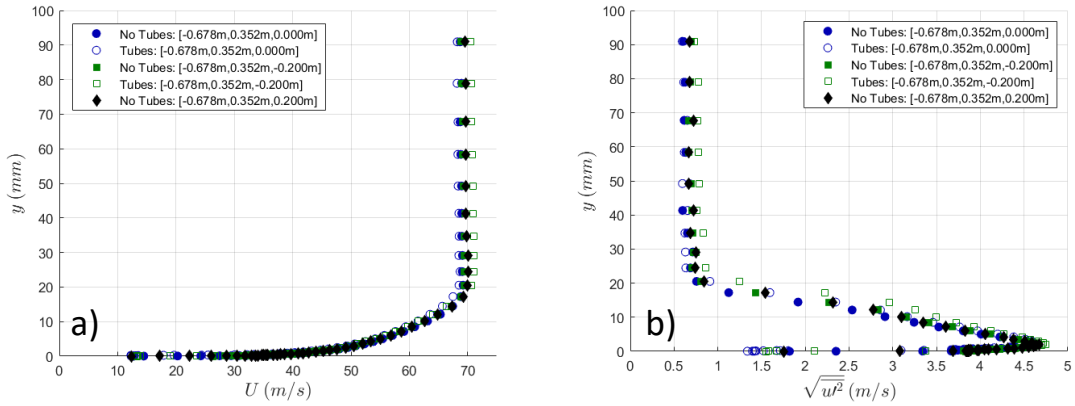

Figure 12 Comparison of incoming mean flow a) and turbulent stress b) boundary layers both with and without the modified seeding tubes installed showing negligible difference in flow condition. Note that the profiles were taken using hot-wire anemometry for the Case A configuration.

Turbulent Boundary Layer (TBL) Development Plate

The boundary layer development plate, shown in Figure 13, spans the full 0.914 m (3 ft) width of the test section, is 1.462 m (57.57 in) in streamwise length and its top surface is lifted 0.352 m (13.88 in) off of the test section floor. It is constructed from 19.1 mm (0.75 in) thick aluminum plating, see Figure 13 c), and secured to the test section floor via 18 steel legs to prevent aeroelastic vibrations, see Figure 13 b). To ensure the incoming boundary layer was turbulent, it was tripped with a 101.6 mm (4 in) wide strip of distributed sand grain roughness with an average roughness element size of 46 μm, mounted 1.2 m (47.2 in) upstream of the ramp leading edge, as shown in Figure 13 a) and d). The plate also contains a streamwise array of static pressure taps (1) in order to characterize the upstream boundary layer pressure gradient conditions. As will be described below, the streamwise pressure gradient can be controlled by a flexible top wall insert.

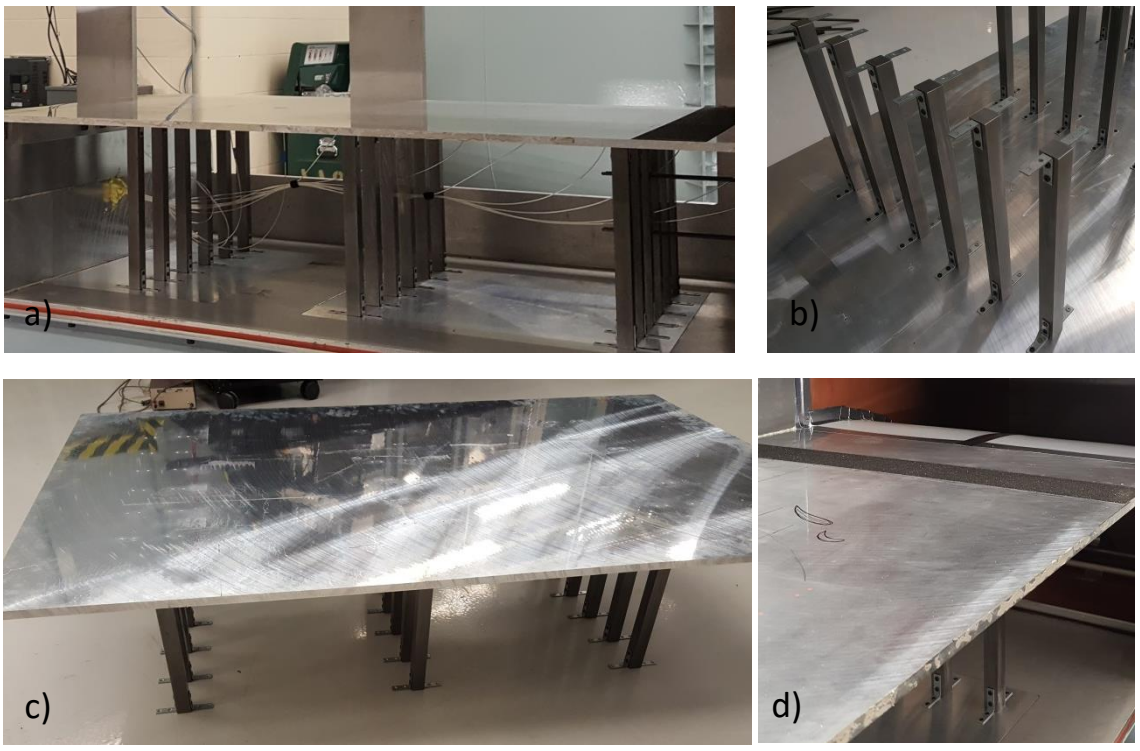

Figure 13 Various views of the boundary layer development plate during the installation process highlighting the aluminum plate c), the steel support legs b), and the tripping roughness element a) and d).

Top Wall Inlet Contour

To transition the flow from the top of the wind tunnel inlet contraction to the flexible top wall insert, a small two-dimensional contour was installed (see Figure 2). Like the ramp geometry, this contour is machined aluminum in the form of a fifth-order polynomial with zero first and second derivative end conditions. It is given by the following parametric form,

$$Y(X) = b_1 + b_2X^3 + b_3X^4 + b_4X^5 \quad for \ [-1.4623 < \mathrm{X} < -1.0813] \tag{3}$$

where X and Y are both in the global coordinate system. The constants are given in terms of the ramp length, L_2 = 0.3810 m, the ramp height, H_2 = 0.0986 m, and the vertical offset, H_{off2} = 0.8158 m, as follows:

$$b_1 = \left(H + H_{off_2}\right), \quad b_2 = -10H_2/L_2^3, \quad b_3 = 15H_2/L_2^4, \quad b_4 = -6H_2/L_2^5 \tag{4}$$

Flexible Top Wall Insert / Turnbuckle Assembly

In order to adjust the streamwise APG over the ramp surface and thereby achieve each of the desired archival benchmark flow cases, a flexible tunnel top wall assembly was designed and installed in the test section. Figure 14 shows a schematic of the flexible upper wall assembly and the associated multiple turnbuckle system that is used to adjust the ceiling contour. The flexible ceiling was constructed from 10-gauge aluminum sheet metal (0.102 in) and is nominally mounted 9.86 cm (3.88 in) below the test section ceiling. The top three windows of the test section were removed, and were replaced with three aluminum blanks, with the turnbuckle assemblies integrated into them as shown in Figure 14. At the test section inlet, the top wall inlet contour

smoothly transitions the flow to the flexible ceiling. It also serves to prevent any flow from passing between the top of the test section and flexible ceiling. The ceiling is nominally positioned 0.46 m above the boundary layer development plate. Adjustments to this nominal position allow the pressure gradient on the boundary layer development plate to vary from initially mildly favorable (due to the both top and bottom internal inlet contractions) to approximately ZPG. Over the convex ramp surface, the adjustment of the turnbuckles allows the desired APG to be imposed on the ramp TBL.

For each APG TBL case the wall contour was carefully measured. To do this the three panels on the test section ceiling that house the turnbuckle adjustment mechanisms also were equipped with access holes for accurately measuring the position of the ceiling. There are 23 holes down the centerline of the test section with holes on each side at five streamwise positions in order to verify spanwise uniformity of the ceiling position. In order to record the flexible ceiling location, a pair of digital calipers is used as a depth gauge to go through each hole to measure the distance between the panel top surface and the flexible ceiling top surface. This measurement is repeated for each of the 33 holes in the tunnel ceiling. Once these measurements are recorded, the holes are sealed in order to prevent any airflow through them. Figure 15 shows the hole positions for each of the three ceiling panels. The number of measurement holes is greatest for the third panel which is located over the convex ramp where wall curvature is greatest.

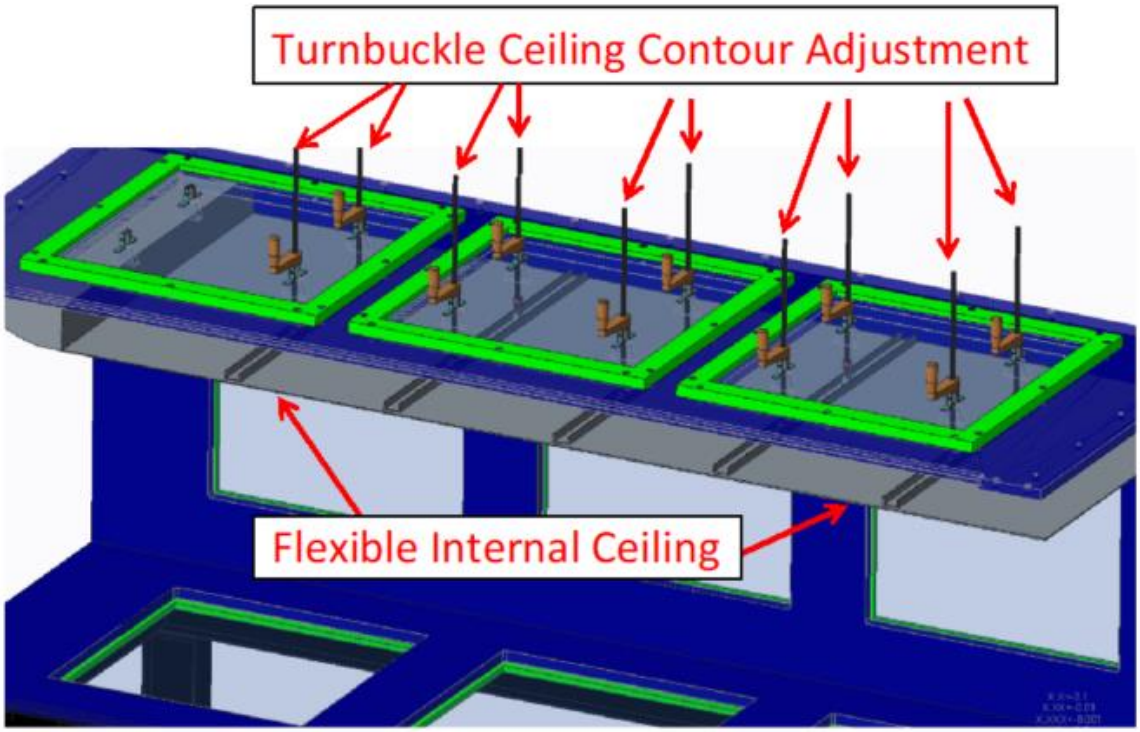

Figure 14 Flexible top wall insert and turnbuckle assembly. Flow is from left to right.

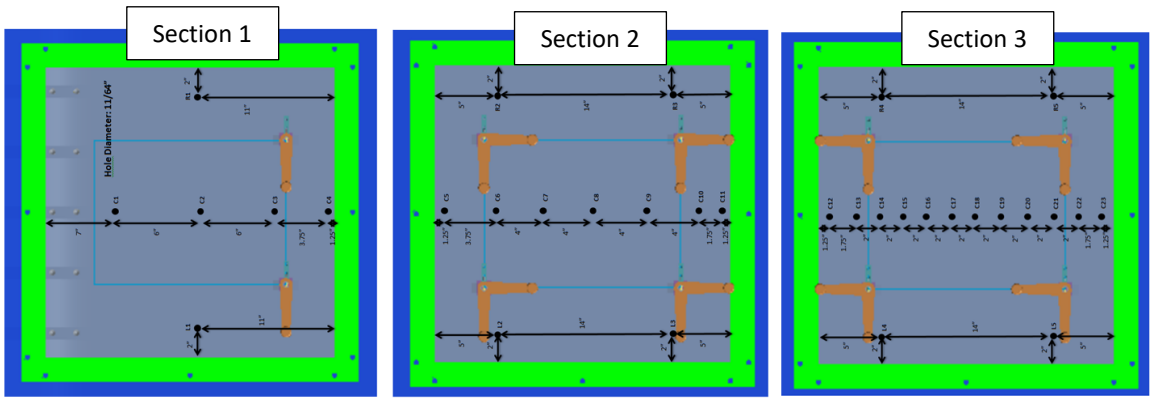

Figure 15 Schematic top view of test section ceiling showing locations for measuring the position of the flexible ceiling contour.

The ceiling position measurements were repeated prior to each test entry and with the changing of separation test cases. Appendix 2 provides tables of the ceiling position measurements, converted to the global coordinate system, for each of these instances. Included in these tables is the mean ceiling position and the estimated uncertainty. The combined standard uncertainty of Y is a combination of the random uncertainty, s_Y, and the systematic standard uncertainty, b_Y.

$$u_Y = [\, b_Y^2 + \, s_Y^2]^{\frac{1}{2}} \tag{5}$$

The random uncertainty, s_Y, is related to the variance as follows:

$$s_Y = \sqrt{\frac{Var(Y)}{N}} \tag{6}$$

where N is the number of times the ceiling configuration was repositioned and measured (4 times for Case A). The systematic uncertainty was divided into three components, the caliper uncertainty, b_c, taken as 0.025 mm (0.001 in), the sheet metal thickness uncertainty, b_t, taken as 0.127 mm (0.005 in), and the uncertainty of the machining of the test section, b_m, taken as 1.270 mm (0.050 in).

$$b_Y = [\, b_c^2 + \, b_t^2 + \, b_m^2]^{\frac{1}{2}} \tag{7}$$

The expanded uncertainty is the combined standard uncertainty multiplied by the Student's t-table value, $t_{v,p}$ where ν is N – 1 and p is the selected confidence interval. At 20:1 odds or p = 95% confidence, $t_{v,p}$ = 3.18 for Case A. Using this analysis, the true value is expected to lie within:

$$Y_{mean} \pm t_{v,p} u_Y \tag{8}$$

where $t_{v,p}\, u_Y$ is the expanded uncertainty or simply the 95% confidence intervals in this case. Note that for Cases C only two repeated measurement sets were taken, so instead of using this value, it was estimated to have the same random uncertainty as Case B.

Diffuser Transition

The end of the flexible internal ceiling is transitioned into the diffuser via a hinged assembly that provides a linear transition from the end of the flexible internal ceiling to the diffuser

ceiling. This transition piece, shown in Figure 16, was necessary on two accounts: (1) it provided additional structural rigidity that prevented vibration of the flexible ceiling, and (2) it eliminated feedback likely to occur via separated flow entering the cavity between the actual test section ceiling and the flexible internal sheet metal ceiling. Due to the fastener location on the diffuser ceiling being fixed, and the end of the flexible internal ceiling being dictated by the required ceiling configuration, the linear section of the hinged assembly had to be custom made for each ceiling configuration. This equated to the lower the ceiling configuration, the longer the linear portion of the hinged assembly.

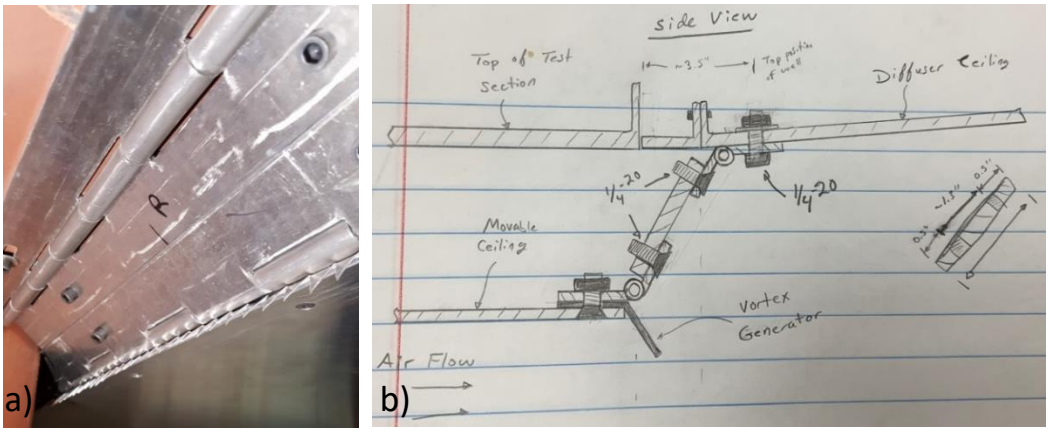

Figure 16 Photograph a) and schematic b) of the diffuser hinged assembly transition piece.

Due to the central cruciform in the diffuser, the hinged assembly was divided into two parts, one for each side of the cruciform. Each side of the hinged assembly consisted of two aluminum piano hinges, a linear section, and a streamwise vortex generator strip, see Figure 17 a). Downstream of the ramp, on the lower part of the test section, the flow smoothly contours into the diffuser via removable inserts.

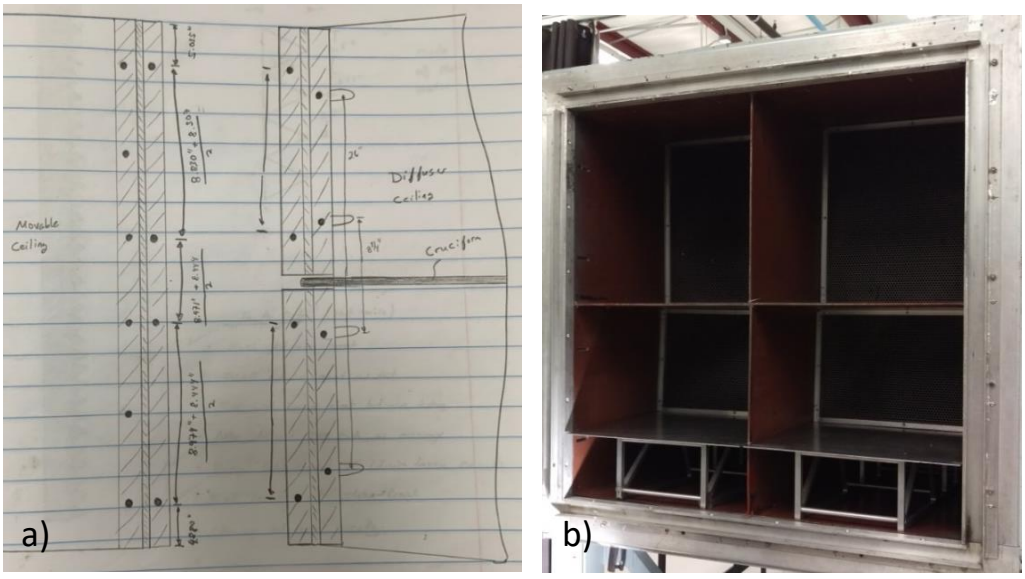

Figure 17 Schematic top view of the piano hinge transition piece showing the diffuser cruciform a), and photograph of the hexagonal grids installed in the diffuser b).

In order to provide a pressure drop, and decouple the upstream and downstream flow, hexagonal mesh grids were installed approximately 0.51 m (20 in) downstream of the test section in each of the 4 sections of the diffuser, see Figure 17 b). Each cell of the hexagonal grids was approximately 6.4 mm (0.25 in) in diameter and in total provided a blockage of approximately 21%.

Adjustable Wind Tunnel Sidewall

A new test section sidewall, located on the wind tunnel outer loop (-Z axis) and not shown in Figure 4, with adjustable window positioning was fabricated to allow complete sidewall optical access at any streamwise location. This new sidewall is shown in part b) of Figure 18 and can be compared to the original sidewall, shown in part a) of Figure 18. In the configuration shown in Figure 18, the window locations for the two sidewalls are at similar streamwise positions; however, the new adjustable sidewall places the windows 51 mm (2.0 in) lower. This can be easily seen by comparing the different widths of the upper and lower crossbars in Figure 18 b). The new adjustable sidewall can also take on different window positions by repositioning the central supports, highlighted in yellow in Figure 18 b), with additional supports and half windows being added as necessary. This setup allowed a special 0.5" thick plate glass window to be positioned anywhere in the central region of the sidewall, which in turn, allowed complete optical access over the ramp geometry, a necessity for the LDV measurements.

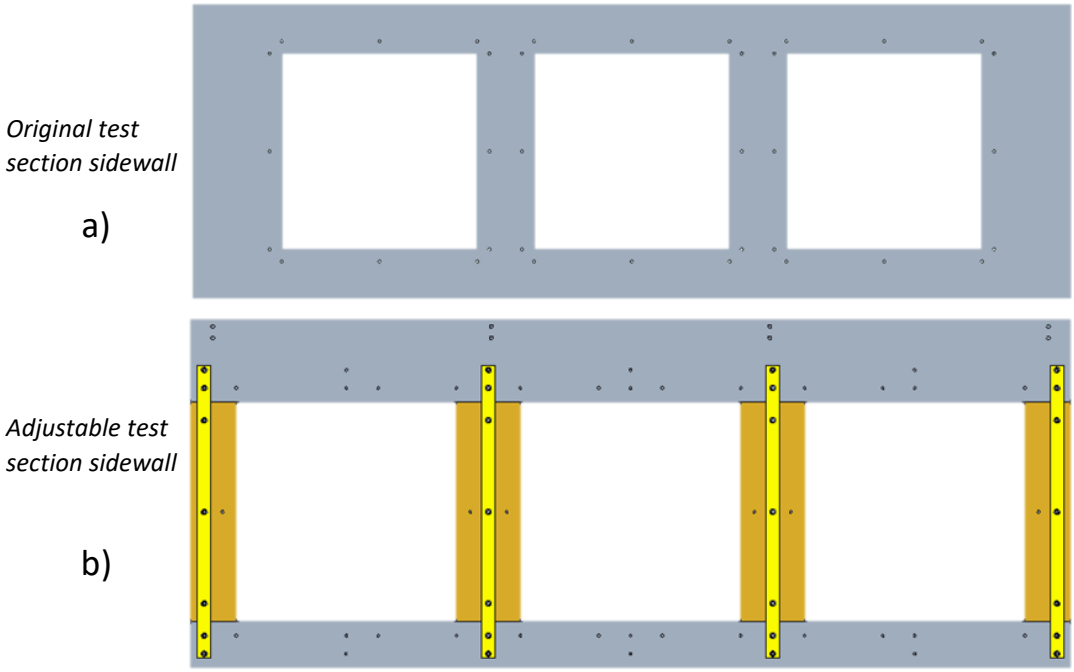

Figure 18 Comparison of original test section sidewall a) and new adjustable sidewall b). Note that the new adjustable sidewall is positioned 51 mm lower and allows the central supports to be repositioned as necessary.

Appendix 1

Table 1 Surface pressure tap center point locations. Units are in meters and are given in the global coordinate system. Tap locations on the boundary layer development plate, ramp model, and recovery region are highlighted by color for ease of reference.

Centerline			Off Centerline		
X (m)	Y (m)	Z (m)	X (m)	Y (m)	Z (m)
-1.4369	0.3524	0	0.03	0.3523	-0.168
-1.3099	0.3524	0	0.03	0.3523	-0.084
-1.1829	0.3524	0	0.03	0.3523	0.084
-1.0559	0.3524	0	0.03	0.3523	0.168
-0.9289	0.3524	0	0.21	0.3351	-0.168
-0.8019	0.3524	0	0.21	0.3351	-0.084
-0.6749	0.3524	0	0.21	0.3351	0.084
-0.5479	0.3524	0	0.21	0.3351	0.168
-0.4209	0.3524	0	0.39	0.2771	-0.168
-0.2939	0.3524	0	0.39	0.2771	-0.084
-0.1669	0.3524	0	0.39	0.2771	0.084
-0.0399	0.3524	0	0.39	0.2771	0.168
0.03	0.3523	0	0.61	0.1911	-0.168
0.05	0.3521	0	0.61	0.1911	-0.084
0.07	0.3516	0	0.61	0.1911	0.084
0.09	0.3507	0	0.61	0.1911	0.168
0.11	0.3494	0	0.79	0.1554	-0.168
0.13	0.3476	0	0.79	0.1554	-0.084
0.15	0.3453	0	0.79	0.1554	0.084
0.17	0.3425	0	0.79	0.1554	0.168
0.19	0.339	0	0.9599	0.1524	-0.168
0.21	0.3351	0	0.9599	0.1524	-0.084
0.23	0.3305	0	0.9599	0.1524	0.084
0.25	0.3254	0	0.9599	0.1524	0.168
0.27	0.3198	0	1.1397	0.1524	-0.168
0.29	0.3137	0	1.1397	0.1524	-0.084
0.31	0.3071	0	1.1397	0.1524	0.084
0.33	0.3001	0	1.1397	0.1524	0.168
0.35	0.2927	0			
0.37	0.285	0			
0.39	0.2771	0			
0.41	0.269	0			
0.43	0.2607	0			
0.45	0.2524	0			
0.47	0.2441	0			
0.49	0.2358	0			
0.52	0.2237	0			

Boundary Layer Development Plate

Ramp Model

Recovery Region

0.55	0.2121	0			
0.58	0.2012	0			
0.61	0.1911	0			
0.64	0.1821	0			
0.67	0.1743	0			
0.7	0.1677	0			
0.73	0.1623	0			
0.76	0.1583	0			
0.79	0.1554	0			
0.82	0.1536	0			
0.85	0.1527	0			
0.88	0.1524	0			
0.8999	0.1524	0			
0.9299	0.1524	0			
0.9599	0.1524	0			
0.9898	0.1524	0			
1.0198	0.1524	0			
1.0498	0.1524	0			
1.0798	0.1524	0			
1.1097	0.1524	0			
1.1397	0.1524	0			
1.1697	0.1524	0			
1.1997	0.1524	0			
1.2296	0.1524	0			

Appendix 2

Table 2 Position of the flexible ceiling for separation Case A. Note that each Y_i is an independent repeated installation and adjustment of the ceiling with Y_{mean} being the average value and that which is most applicable to describe the ceiling location.

Flexible Ceiling Position for Separation Case A								
Section 1								
Location #	X (m)	Z (m)	Y_1 (m)	Y_2 (m)	Y_3 (m)	Y_4 (m)	Y_{mean} (m)	$Y_{CI\_95\%}$ (m)
L1	-0.853	0.254	0.818	0.818	0.818	0.818	0.818	0.004
R1	-0.853	-0.254	0.820	0.820	0.820	0.820	0.820	0.004
C1	-1.005	0.000	0.817	0.817	0.817	0.817	0.817	0.004
C2	-0.853	0.000	0.819	0.819	0.819	0.819	0.819	0.004
C3	-0.700	0.000	0.822	0.822	0.822	0.822	0.822	0.004
C4	-0.605	0.000	0.824	0.824	0.824	0.824	0.824	0.004
Section 2								
L2	-0.269	0.254	0.828	0.825	0.826	0.827	0.827	0.005
L3	0.087	0.254	0.822	0.818	0.819	0.821	0.820	0.005

R2	-0.269	-0.254	0.819	0.827	0.826	0.827	0.825	0.007
R3	0.087	-0.254	0.817	0.821	0.820	0.820	0.820	0.005
C5	-0.364	0.000	0.825	0.826	0.826	0.826	0.826	0.004
C6	-0.269	0.000	0.826	0.826	0.826	0.826	0.826	0.004
C7	-0.167	0.000	0.826	0.826	0.826	0.826	0.826	0.004
C8	-0.065	0.000	0.824	0.824	0.826	0.825	0.825	0.004
C9	0.036	0.000	0.822	0.821	0.823	0.823	0.822	0.004
C10	0.138	0.000	0.816	0.817	0.817	0.818	0.817	0.004
C11	0.182	0.000	0.814	0.814	0.815	0.816	0.815	0.004
Section 3								
L4	0.519	0.254	0.790	0.791	0.792	0.793	0.791	0.005
L5	0.875	0.254	0.769	0.770	0.771	0.771	0.770	0.004
R4	0.519	-0.254	0.795	0.795	0.794	0.794	0.794	0.004
R5	0.875	-0.254	0.772	0.769	0.772	0.772	0.771	0.005
C12	0.424	0.000	0.799	0.799	0.799	0.800	0.799	0.004
C13	0.468	0.000	0.796	0.796	0.796	0.797	0.796	0.004
C14	0.519	0.000	0.792	0.793	0.793	0.793	0.793	0.004
C15	0.570	0.000	0.789	0.790	0.790	0.790	0.790	0.004
C16	0.621	0.000	0.786	0.786	0.787	0.786	0.786	0.004
C17	0.671	0.000	0.783	0.783	0.784	0.783	0.783	0.004
C18	0.722	0.000	0.780	0.780	0.781	0.780	0.780	0.004
C19	0.773	0.000	0.777	0.777	0.778	0.777	0.777	0.004
C20	0.824	0.000	0.774	0.774	0.775	0.775	0.775	0.004
C21	0.875	0.000	0.771	0.771	0.772	0.771	0.771	0.004
C22	0.925	0.000	0.768	0.768	0.768	0.768	0.768	0.004
C23	0.970	0.000	0.766	0.765	0.764	0.766	0.765	0.004
End	1.281	0.000	0.749	0.749	0.749	0.749	0.749	0.004

Table 3 Position of the flexible ceiling for separation Case B. Note that each Y_i is an independent repeated installation and adjustment of the ceiling with Y_{mean} being the average value and that which is most applicable to describe the ceiling location.

Flexible Ceiling Position for Separation Case B							
Section 1							
Hole #	X (m)	Z (m)	Y_1 (m)	Y_2 (m)	Y_3 (m)	Y_{mean} (m)	$Y_{CI\_95\%}$ (m)
L1	-0.853	0.254	4.188	4.201	4.202	4.197	0.006
R1	-0.853	-0.254	4.132	4.140	4.132	4.135	0.006
C1	-1.005	0.000	4.280	4.250	4.250	4.260	0.006
C2	-0.853	0.000	4.148	4.154	4.151	4.151	0.006
C3	-0.700	0.000	4.300	4.043	4.043	4.129	0.006
C4	-0.605	0.000	3.966	3.986	3.981	3.978	0.006

Section 2							
L2	-0.269	0.254	3.778	3.855	3.845	3.826	0.008
L3	0.087	0.254	4.148	4.240	4.306	4.231	0.007
R2	-0.269	-0.254	3.877	3.854	3.855	3.862	0.006
R3	0.087	-0.254	4.226	4.271	4.252	4.250	0.006
C5	-0.364	0.000	3.848	3.868	3.921	3.879	0.006
C6	-0.269	0.000	3.828	3.855	3.892	3.858	0.006
C7	-0.167	0.000	3.853	3.884	3.918	3.885	0.006
C8	-0.065	0.000	3.928	3.977	3.992	3.966	0.006
C9	0.036	0.000	4.106	4.134	4.150	4.130	0.006
C10	0.138	0.000	4.404	4.418	4.455	4.426	0.006
C11	0.182	0.000	4.590	4.594	4.581	4.588	0.006
Section 3							
L4	0.519	0.254	6.214	6.155	6.192	6.187	0.006
L5	0.875	0.254	7.422	7.464	7.447	7.444	0.006
R4	0.519	-0.254	6.111	6.065	6.115	6.097	0.006
R5	0.875	-0.254	7.351	7.403	7.424	7.393	0.006
C12	0.424	0.000	5.722	5.714	5.736	5.724	0.006
C13	0.468	0.000	5.888	5.902	5.907	5.899	0.006
C14	0.519	0.000	6.109	6.103	6.094	6.102	0.006
C15	0.570	0.000	6.308	6.303	6.303	6.305	0.006
C16	0.621	0.000	6.497	6.477	6.536	6.503	0.006
C17	0.671	0.000	6.670	6.713	6.700	6.694	0.006
C18	0.722	0.000	6.850	6.865	6.889	6.868	0.006
C19	0.773	0.000	7.020	7.036	7.054	7.037	0.006
C20	0.824	0.000	7.182	7.212	7.235	7.210	0.006
C21	0.875	0.000	7.374	7.420	7.420	7.405	0.006
C22	0.925	0.000	7.586	7.650	7.626	7.621	0.006
C23	0.970	0.000	7.786	7.852	7.826	7.821	0.006
End	1.281	0.000	9.154	9.154	9.154	9.154	0.006

Table 4 Position of the flexible ceiling for separation Case C. Note that each Y_i is an independent repeated installation and adjustment of the ceiling with Y_{mean} being the average value and that which is most applicable to describe the ceiling location.

Flexible Ceiling Position for Separation Case C						
Section 1						
Hole #	X (m)	Z (m)	Y_1 (m)	Y_2 (m)	Y_{mean} (m)	$Y_{CI\_95\%}$ (m)
L1	-0.853	0.254	4.188	4.208	4.198	0.006
R1	-0.853	-0.254	4.132	4.138	4.135	0.006
C1	-1.005	0.000	4.248	4.257	4.253	0.006
C2	-0.853	0.000	4.148	4.154	4.151	0.006
C3	-0.700	0.000	4.011	4.046	4.029	0.006

C4	-0.605	0.000	3.950	3.981	3.966	0.006
Section 2						
L2	-0.269	0.254	3.817	3.859	3.838	0.006
L3	0.087	0.254	4.359	4.405	4.382	0.006
R2	-0.269	-0.254	3.867	3.839	3.853	0.006
R3	0.087	-0.254	4.347	4.339	4.343	0.006
C5	-0.364	0.000	3.906	3.913	3.910	0.006
C6	-0.269	0.000	3.832	3.886	3.859	0.006
C7	-0.167	0.000	3.879	3.831	3.855	0.006
C8	-0.065	0.000	3.946	3.954	3.950	0.006
C9	0.036	0.000	4.175	4.177	4.176	0.006
C10	0.138	0.000	4.589	4.646	4.618	0.006
C11	0.182	0.000	4.867	4.928	4.898	0.006
Section 3						
L4	0.519	0.254	7.119	7.091	7.105	0.006
L5	0.875	0.254	8.747	8.687	8.717	0.006
R4	0.519	-0.254	6.911	6.976	6.944	0.006
R5	0.875	-0.254	8.687	8.688	8.688	0.006
C12	0.424	0.000	6.400	6.523	6.462	0.006
C13	0.468	0.000	6.677	6.670	6.674	0.006
C14	0.519	0.000	6.965	6.988	6.977	0.006
C15	0.570	0.000	7.246	7.247	7.247	0.006
C16	0.621	0.000	7.509	7.491	7.500	0.006
C17	0.671	0.000	7.790	7.707	7.749	0.006
C18	0.722	0.000	7.973	7.931	7.952	0.006
C19	0.773	0.000	8.206	8.154	8.180	0.006
C20	0.824	0.000	8.453	8.371	8.412	0.006
C21	0.875	0.000	8.710	8.631	8.671	0.006
C22	0.925	0.000	8.976	8.993	8.985	0.006
C23	0.970	0.000	9.208	9.356	9.282	0.006
End	1.281	0.000	11.154	11.279	11.217	0.006